Self-diffusion effects in micro scale liquids. Numerical study by a dissipative particle dynamics method

J. CZERWIŃSKA*

Institute of Fundamental Technological Research, Polish Academy of Science, 21 Świętokrzyska St., 00-049 Warsaw, Poland

Abstract. Mesoscale flows of liquid are of great importance for various nano- and biotechnology applications. Continuum model do not properly capture the physical phenomena related to the diffusion effects, such as Brownian motion. Molecular approach on the other hand, is computationally too expensive to provide information relevant for engineering applications. Hence, the need for a mesoscale approach is apparent. In recent years many mesoscale models have been developed, particularly to study flows of gas. However, mesoscale behaviour of liquid substantially differs from that of gas. This paper presents a numerical study of micro-liquids phenomena by a Voronoi Dissipative Particle Dynamics method. The method has its origin from the material science field and is one of very few numerical techniques which can describe correctly molecular diffusion processes in mesoscale liquids. This paper proves that correct prediction of molecular diffusion effects plays predominant role on the correct prediction of behaviour of immersed structures in the mesoscopic flow.

Key words: micro- and nanofluidics, mesoscale simulations.

1. Introduction

Reynolds number defines the characteristic of the fluid flow for the continuum medium. If the compressibility of the gas was neglected, then gas and liquid can be treated in similar way. However, from the molecular point of view, the two fluids behave very differently. The average distance between gas molecules is at least one order of magnitude higher than in liquids. The interaction in gases is mostly defined by bilateral collisions. In contrary, liquid molecules are tightly packed and they interact by intermolecular potential causing cohesion of liquids. Hence, the differences between behaviour of liquids and gasses will appear in mesoscale and this leads to requirement for a different theoretical and numerical treatments of the two media. In the last few years, the research interest had been mostly focused on modelling of micro-flow of gases. Some examples are presented in [1] and [2]. However, the increasing interest in understanding of bio-processes and the development of bioengineering requires more comprehensive study of mesoscale behaviour of liquids. Hence, the present paper will focus on a new numerical development applicable to liquids.

The question that naturally arises first would be the definition of mesoscale. For gases Knudsen number, based on the molecular mean free path, helps to define boundaries. Cohesion of liquids, however, makes a counterpart parameter difficult to define. Solids, similarly to liquids, are also characterized by cohesion. Molecules in solids remain localized in the vicinity of the equilibrium lattice position (rigidity of solids), and will very rarely jump between neighbours. In liquids molecules will drift apart.

Einstein relation describes the mean square displacement at time t of the molecule from the initial point in time $t = 0$

$$< |\mathbf{x}(t) - \mathbf{x}(0)|^2 > = 6\,D\,t, \qquad (1)$$

where D – is self-diffusion parameter. Molecular diffusion is the consequence of the thermal fluctuation and a property of irreversibility. In contrary to viscous flow, molecular diffusion appear spontaneously without presence of external forces, and for liquid, it is typically of the order of $D \sim 10^{-9} m^2/s$. The difference between solids and liquids, which manifests itself in the molecular drift processes, helps estimate one border of the mesoscale description. Due to the fact that molecular diffusion is not limited by any space or time restriction, this property will define the upper-bond of the mesoscale. Thermal fluctuations effects (Brownian motion) are prominent on the scale of the order of micro- and nano-meters. However, on the larger scale and for very long time, the process can be averaged and neglected.

The lower limit of the mesoscale can be derived from the differences between gas and liquid at the molecular level. The radial distribution function $g(\mathbf{r})$ is a quantitative measure of molecular order. It provides the information about the local density $\rho(\mathbf{r})$ of molecules around a given molecule. Figure 1 shows radial distribution function for a gas and a liquid. Gas molecules are sparse and bilateral collisions determined transport processes between them. However, liquids on the molecular level are very different. The radial distribution function has several local maxima. This means that behaviour of the single molecule is influenced by the closer and also by the rela-

---

*e-mail: jczer@ippt.gov.pl

tively distant neighbours. The size of the molecules as well as the strength of the interaction will be limiting factor of various liquid behaviour. Several maxima in radial distribution function can explain the self-organization and clustering mechanism, which occur on the order of nano-meter scale, as illustrated in [3]. By changing the size of liquid molecules (polymers, complex molecules in [4]) and the strength of interaction (electro-magnetic field in [5]) molecular effects beyond the nano-meter scale have to be consider. Non-Newtonian behaviour of some liquids is one of the effect connected with the intermolecular scale length. For most common liquids the changes in these effects start to be noticeable on the order of few nano-meters and on the larger scale inter particle interactions phenomena in liquids are similar to the continuum description. Hence, the intermolecular interaction provides guidelines for the definition of the lower bound of the mesoscale.
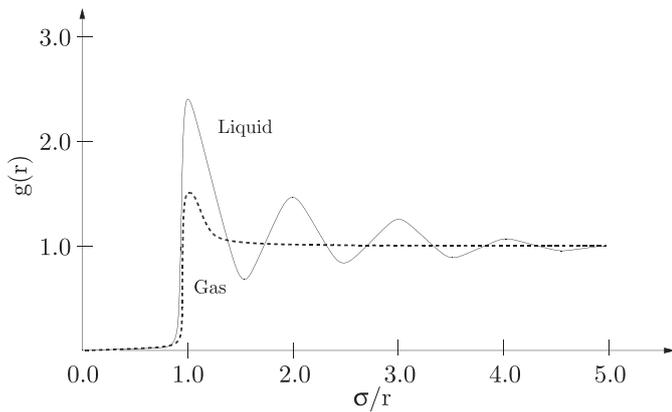

Fig. 1. Sketch of typical radial distribution function $g(\mathbf{r})$ for a gas and a liquid; σ is the size of the molecule. In liquids molecules are tightly packed. Hence, the presence of several local maxima in the radial distribution function

Concluding, cohesion and molecular drift in liquids allow the definition of limits on the scale, which later herein will be referred to as a mesoscale. Molecular description (microscale) is limited by the relevance of the time and space scales related to the changes in the inter particle potential effects. This describes lower bound of the mesoscale. The continuum approach (macroscale) has its lower bound limited by the influence of the thermal fluctuation phenomena and it provides upper limit of the mesoscale. Various phenomena important for the bio- and nanotechnology are taking place in such defined mesoscale regime. Examples in [6–8]. Due to that fact there is a need for efficient and accurate simulation techniques which will enhance understanding of mesoscale processes in liquids as well as provide help in designing micro-devices.

2. Fundamental physics of the mesoscale liquids

The borders of the mesoscale have been defined in introduction section. The lower bound of the scale is es-

tablished by short range changes in intermolecular force interaction. However, the interaction is very complex in nature and can represent itself in various ways. Neglecting the possible electromagnetic effects the following phenomena are related to the intermolecular potential:

1) interaction between the same fluid molecules – viscous effects;
2) interaction between molecules of different fluids – immiscibility, surface tension;
3) interaction between fluid and solid molecules – slip or no-slip phenomena;
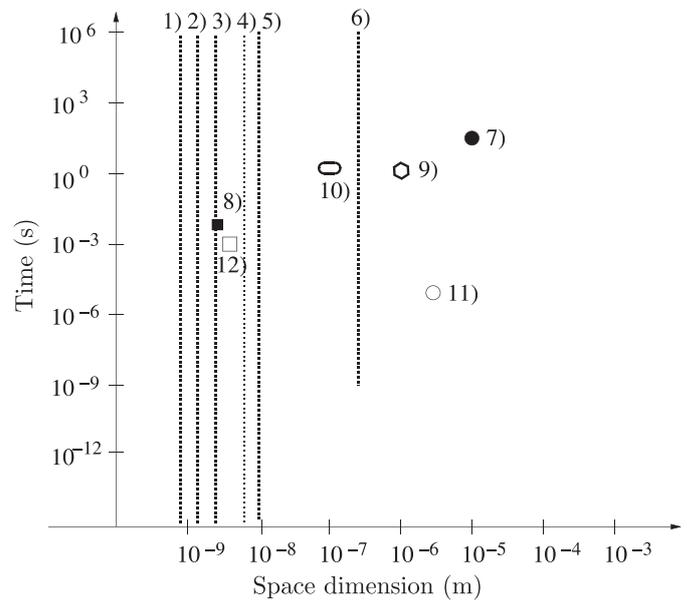4) interaction between two fluids and solid molecules – wetting phenomena.

Fig. 2. Diagram represents comparison of important time and space scales for liquids. The lines indicate that the considered phenomenon is time dependent on the scale of the order of femto-seconds, therefore time influence can be neglected; points refer to the specific time and space occurrence of the phenomenon. Indexes on figure represent as follow: 1) Molecular Dynamics study of changes in the surface tension due to the thermal fluctuations (0.9 nm) in [9]; 2) Molecular Dynamics slip effects in binary mixtures ($\sim$ 2 interaction lengths, 2 nm) in [10]; 3) Molecular Dynamics study of the effect of the roughness of the surface on the viscosity of the film (3.89 nm) in [11]; 4) Molecular Dynamics study of the effect of the length of the molecule on the slip (7.9 nm) in [11]; 5) Molecular Dynamics study of the solid-fluid interface boundary condition (up to 10nm) in [12]; 6) Charged colloidal suspension nucleation, self organized structures (320 nm) in [13]; 7) DNA fluctuations (DNA length - 10μm) in [14]; 8) *Ecoli* RNA fluctuations in [15]; 9) Colloidal hard spheres suspension in [16]; 10) DNA fluctuations (DNA length - 0.1μm) in [17]; 11) Brownian particles in polymer solutions in [18]; 12) Brownian motion of yeast cell walls in [19]

Figure 2 shows experimental and numerical data for various effects in the mesoscale liquids. The phenomena related to the intermolecular forces are generally not time dependant (if time scale is larger than femto-seconds),

therefore are marked as a straight lines. The intermolecular processes have to be described by microscale (atomistic) models in the range of several nano-meters. Larger scales do not require such modelling and continuum approach is sufficient. The second type of phenomena related to molecular drift will, however, show their strength depending on the time and space scale of the problem considered. For complex fluidics such as polymers or colloids it can be noticeable up to few millimetres. Figure 2 shows the molecular diffusion effects by dots. Majority of effects will appear as a Brownian motion of immersed structures in the flow. It can be noted that some of the data (7–10,12) are correlated as straight line, with the slope being of the value of the order of the water diffusion coefficient. Point (11) consider complex polymer colloids. Hence, molecular diffusion coefficient differs.

In summary, Fig. 2 provides the guideline in deciding the modelling approach for mesoscale liquids. If the flow phenomena were of the scale larger than several nano-meters, molecular potential interaction is well described by continuum equations. Molecular drift effects however are significant and present on the larger scales. Some phenomena such as Brownian motion or molecular mixing are examples of molecular drift related effects and can show the influence on various space and time scales. Thus, the time scale difference in which the intermolecular forces and self-diffusion phenomena achieve equilibrium state defines the upper border of the mesoscale. The Schmidt number

$$Sc = \frac{\nu}{D} \qquad (2)$$

represents relation of viscous effects (ν -viscosity of fluid) to the mass transfer effects (D self-diffusion). Large Sc (typically for water ~ 1000) indicate that the equilibrium state related to the viscous effects is obtained much faster than the one corresponding to the molecular drift processes. Another way to estimate space and time relation limiting mesoscale physical effects is to define quantity similar to the Mach number

$$M = \frac{s/t}{a}, \qquad (3)$$

where a is speed of sound and instead of the flow velocity the space s and time t relation of considered problem is present. The speed of sound defines the speed of propagation of small disturbances in the medium. This can be related on more fundamental atomic level to the fluctuations, example in [20]. Hence if the space and time relation for a considered problem leads to $M \sim 1$, small disturbances effects will influence the flow. As it can be noted in the characteristic space/time relation from equation 1 and from equation 3 for water are of the similar order $(7.7 \cdot 10^{-5} - 8.3 \cdot 10^{-4} m/s)$. Thus, for some circumstances such define Mach number maybe easier to estimate than local Schmidt number.

Molecular diffusion will be the predominate factor differentiating meso- and macroscale. Hence, the numeri-

cal approach to model mesoscale liquids has to describe molecular diffusion processes correctly.

3. Numerical methods and coarse graining procedure

Mesoscale numerical modelling of liquids requires different approach from the continuum or molecular simulations. Continuum models do not take to account fundamental phenomenon relevant on such scales such as random molecular drift. Molecular simulation, example Molecular Dynamics in [21], conceptually also have several other limitations. The first of which lies in the reliance of computational part. With the fastest computers to date, the number of liquid molecules reach about 10^{-14} of Avogadro number. Hence, Molecular Dynamics describes very small volume of liquid. The second limitation, as indicated by [22], rest on the molecular diffusion process itself and the question, if they can be correctly represented by Molecular Dynamics. Thus, restrictions indicate that more visible approach is to perform some types of coarse graining procedure. This can be achieved in several ways. The most common of which increase the time and space scales by simplification of interaction properties - Lattice Boltzmann Method in [23]. Generally molecular diffusion effects are neglected, however some variations of the Lattice Boltzmann Method allow fluctuation part, example in [24]. Due to the fact, that the motion is restricted to the rigidity lattice certain difficulties arise such as Galilean invariance problem. An alternative approach to coarse graining procedure is to treat the particle as a mesoscopic object interacting with prescribed interaction - Dissipative Particle Dynamics. The degrees of freedom, which are lost during the coarse graining process, are compensated by a respective random forces. This approach will be presented here and will be described in more details in the next section.

4. Dissipative Particle Dynamics formulation

The Dissipative Particle Dynamics was originally proposed by Hoogerbrugge and Koelman [25] as a combination of Lattice Gas Simulation and Brownian Dynamics. The method is based on the modification of Molecular Dynamics potential (Lennard-Jones type) from hard spheres to the soft repulsion. This alternation allowed to make larger time steps possible. However, the removal of the hard core has lead to the drawbacks in modelling viscous effects in fluids. The hard core is responsible for the caging effect. It means that a particle encounters many collisions before it is transported (similarly like in real fluids). The soft repulsion increases significantly (about 1000 times in [27]) mobility of the particles. The Schmidt number is Sc ~ 1. This implies that viscous time scale is comparable with the diffusion time scale. Thus, the method is very inefficient for viscous flows and simulations

require averaging over significant number of time steps, example in [28] and [29]. Lowe [30] proposed modification, which allows flow field modelling more efficiently, by using Maxwellian distribution to strictly control temperature and velocity is sampled by Andersen Monte Carlo thermostat. This leads to significantly higher viscosity of fluids, hence any Schmidt number can be simulated. However, the low viscosity case becomes difficult to obtain using this method. Another drawback of the classical Dissipative Particle Dynamics formulation is that it does not include energy equation, thus certain processes cannot be properly modelled. Bonet Avalos and Mackie [31] proposed altered Dissipative Particle Dynamics with energy conservation, however the same problem considering Schmidt number is present and in this case velocity sampling termostat cannot be used. Several other limiting factors of classical Dissipative Particle Dynamics need to be mentioned. A small Schmidt number indicates that the speed of the propagation of the small disturbances is invalid (speed of sound is much lower). This will manifest itself in the high speed flows, where the shock wave occurs for much lower speeds than in real fluids, but also, it is very important for micro-fluidics. The amplitude of Brownian motion will be much larger that the one of the real fluids. Consequently, the average of the flows with immersed structures are not properly captured. Moreover, the time scale of the Brownian motion for non-equilibrium effects will be incorrect. As it was mentioned earlier, these very phenomena are of the great interest for micro-fluidics applications. Next inconvenience is related to the fact that all dissipative particles are of the same size. The simulation of the effects which require various length scales are restricted by the smallest scale. Hence, this may lead to very large number of particles. Finally another inconvenience is connected with the implementation of boundary condition. The soft potential allows penetration of a boundary. The introduction of the frozen layer of particles helps in establishing the no-slip wall boundary condition, however it causes clustering of the particles near the boundary. This represents itself as a large density fluctuations in the vicinity of the wall (of the order of the value itself in [28]).

The alternative approach to model fluid is to describe a set of volume particles. The origin of this approach is in the Lagrangian solvers for visco-elastic fluids proposed by [32]. Moving Voronoi mesh describes fluid flow based on the Navier-Stokes equations. This approach is sufficient, as it was mentioned earlier, to represent all the intermolecular related processes (such as viscosity, thermal conductivity). However, molecular drift effects are not taken into account. Hence, additionally fluctuating term has been added to ensure a correct value of the molecular diffusion coefficient. Such formulation has various advantages. For example it ensures that the Schmidt number is similar to that of the real fluids. Moreover, the wall boundary condition can be modelled correctly. There is no density jump on the wall.
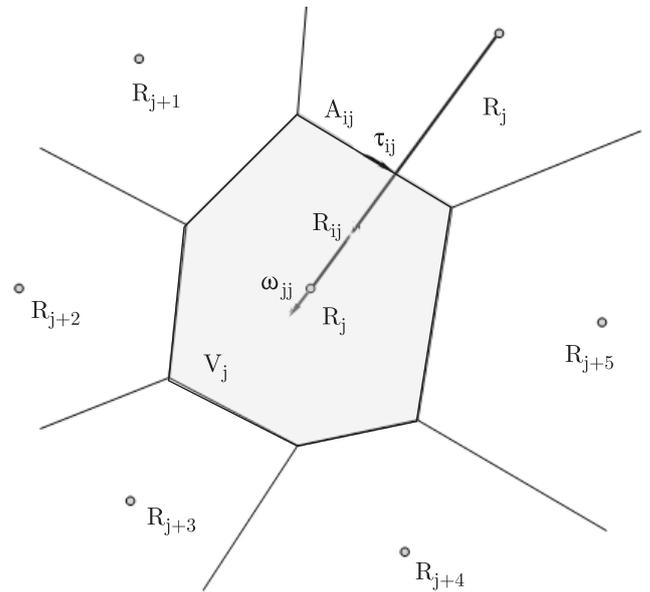

Fig. 3. Voronoi cell i and the quantities defining the discretisation algorithm; A_{ij} - length of the edge ij; $\mathbf{R}_{ij}$ – distance between two particles centres; τ_{ij} – vector defining changes between mass centre of particles ij and the edge centre; ω_{ij} – normalized vector indicating relative movement of the centres of the particles ij; V_i – volume of the particle

Several ways of the derivation of the equations can be found: bottom-up approach in [33] and [34] and top-down derivation in [35,36].

4.1. Basic description – continuum terms. The dissipative particle will be defined as a Voronoi cell. Consequently, space can be divided completely into conjuncted cells. The density of the particle, in contrary to classical Dissipative Particle Dynamics, will be associated with particle volume and can be defined as

$$\rho_i \equiv \frac{1}{V_i} \int_{V_t} d\mathbf{r} \, \rho(\mathbf{r}), \qquad (4)$$

where particle volume is given by relation

$$V_i \equiv \int_{V_t} d\mathbf{r}. \qquad (5)$$

To discretise a continuum equation into the Voronoi cell some additional assumptions are needed.

The average of any variable Q is:

$$[Q]_i \equiv \frac{1}{V_i} \int_{V_t} d\mathbf{r} \, Q(\mathbf{r}). \qquad (6)$$

Following above approximation gradient of variable can be written as

$$[\nabla Q]_i = \frac{1}{V_i} \sum_j \mathbf{\Omega}_{ij} [Q]_j, \qquad (7)$$

where vector $\mathbf{\Omega}_{ij}$ is related to the inter particle mass centre rotation and is given by equation

$$\mathbf{\Omega}_{ij} \equiv \frac{1}{2} A_{ij} \, \omega_{ij}. \qquad (8)$$
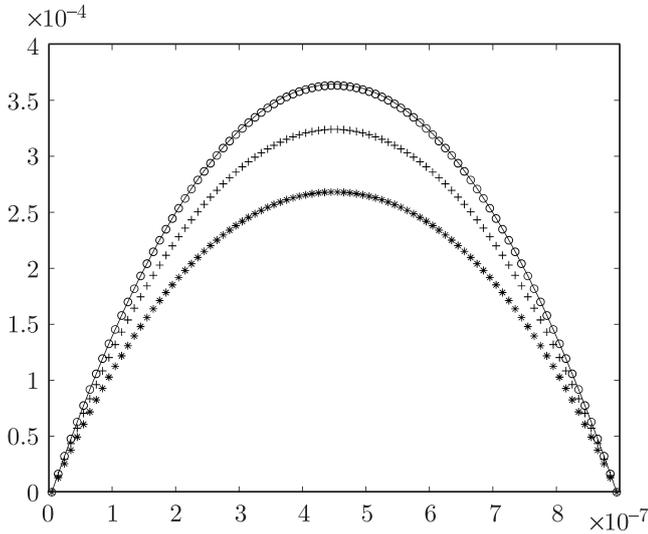
Fig. 4. Channel flow. Time evolution of velocity profile; stars – 4000 time step, crosses – 8000 time steps, circles – 15000, 30000 time steps, straight line – parabola $-1.81 \cdot 10^9 (x - 5 \cdot 10^{-9})(x - 8.95 \cdot 10^{-9})$. The axes correspond: x-coordinate corresponding to channel width in [m], y-velocity in [m/s]

The A_{ij} is the length of the edge between particles i and j, and

$$\omega_{ij} = \frac{\mathbf{R}_{ij}}{A_{ij}}, \tag{9}$$

is related to the relative movement of the Voronoi centres. For any polygon it can be seen that

$$\sum_j A_{ij} \omega_{ij} = 0. \tag{10}$$

Second operator needed for discretisation of continuum equations is convection term

$$\frac{\partial Q}{\partial t} = -\nabla Q \mathbf{v}. \tag{11}$$

This can be approximated from the Eulerian dynamics approach (discrete Gaussian theorem)

$$\frac{d(V_i[Q]_i)}{dt} = -\sum_j \mathbf{\Omega}_{ij}[Q \mathbf{v}]_j, \tag{12}$$

or Lagrangian if

$$\dot{\mathbf{r}}_i = [\mathbf{v}]_i, \tag{13}$$

then it can be proven that

$$\frac{d(V_i[Q]_i)}{dt} = \sum_j \mathbf{\Gamma}_{ij}\overline{[Q]}_{ij}, \tag{14}$$

where

$$\overline{[Q]}_{ij} = \frac{1}{2}([Q]_i + [Q]_j), \tag{15}$$

and

$$\mathbf{\Gamma}_{ij} = \frac{A_{ij}}{R_{ij}} \tau_{ij} ([\mathbf{v}]_i - [\mathbf{v}]_j). \tag{16}$$

Following above definition the continuum equations can be discretise as follow.

Conservation of mass

$$\frac{\partial \rho}{\partial t} = -\nabla \rho \mathbf{v} \tag{17}$$

only requires the convection operator and can be written as

$$\frac{dM_i}{dt} = \frac{d(V_i[\rho]_i)}{dt} = \sum_j \mathbf{\Gamma}_{ij}\overline{[\rho]}_{ij} \tag{18}$$

The momentum equation in discretised form looks as follow

$$\frac{dP_i}{dt} = \frac{d(V_i[\rho \mathbf{v}]_\mathbf{i})}{dt} = \sum_j \mathbf{\Gamma}_{ij}[\overline{\rho \mathbf{v}_{ij}}]$$
$$- \sum_j \mathbf{\Omega}_{ij}([p]_j + \overline{\mathbf{\Pi}}_j + tr\Pi_j \mathbf{1}), \tag{19}$$

where $\overline{\mathbf{\Pi}}$ is symmetric part and $tr\Pi$ is trace of the stress tensor. The entropy equation is as follows

$$\frac{dS_i}{dt} = \sum_j \mathbf{\Gamma}_{ij}\overline{[s]}_{ij} + \frac{1}{T_i}\sum_j \mathbf{\Omega}_{ij}[\mathbf{J}_q]_j$$
$$+ \frac{2\eta_i}{T_i V_i}\overline{\mathbf{G}}_i : \overline{\mathbf{G}}_i + \frac{\zeta_i}{T_i V_i}D_i^2, \tag{20}$$

where $\overline{\mathbf{G}}$ is traceless velocity gradient tensor, D – is the divergence of velocity, η – shear viscosity, ζ – bulk viscosity.

To complete a description the fluctuation part needs to be added. Öttinger [37] proposed the way to add fluctuation in the thermodynamically consistent way. This leads to the following equations for the momentum part:

$$d\mathbf{P}_i^r = \sum_j \mathbf{\Omega}_{ij} \cdot \left(\frac{4\,k_B\,T_j\,\eta_j}{V_j}\right)^{1/2} \overline{d\mathbf{W}_j}$$
$$+ \sum_j \mathbf{\Omega}_{ij} \cdot \frac{1}{2}\left(\frac{4\,k_B\,T_j\,\xi_j}{V_j}\right)^{1/2} tr[d\mathbf{W}_j], \tag{21}$$

and for the entropy

$$dS_i^r = \frac{1}{T_i}\sum_j \mathbf{\Omega_{ij}} \cdot T_j \left(\frac{2k_B\kappa_j}{V_j}\right)^{1/2} d\mathbf{U}_j$$
$$- \frac{1}{T_i}\left(\left(\frac{4k_BT_i\eta_i}{V_i}\right)^{1/2}\overline{d\mathbf{W}_i} + \frac{1}{2}\left(\frac{4k_BT_i\xi_i}{V_i}\right)^{1/2} tr[d\mathbf{W}_j]\right)$$
$$: \sum_j \mathbf{\Omega}_{ji}\mathbf{v}_j^T, \tag{22}$$

where is $\mathbf{U}$ is independent Wiener vector and matrix

$$d\overline{\mathbf{W}}_j = \frac{1}{2}\left(d\mathbf{W}_j + d\mathbf{W}_j^T\right) - \frac{1}{2}tr[d\mathbf{W}_j]\mathbf{1}, \tag{23}$$

is a matrix of independent Wiener processes.

5. Mesoscale physics in simulations

The mesoscale physics described previously needs to be correctly resolved in a numerical simulation. Hence, several issues have to be considered. Firstly, the effects related to the intermolecular potential should be resolved

properly. As it was noted above for the space scale larger than 10 nm the continuum approach for such effects is sufficient and consistent with experiments. Therefore, as a validation the simulation for the Poiseuille flow was performed. For all calculations, the chosen liquid was water. To estimate the parameters of the liquid such as a mass of one particle the assumption was made that the distance of the molecules of water in 2-D dissipative particle is the same as in the normal conditions in 3-D volume. From that specific number of molecules was calculated. The channel size was 1500 nm length and 900 nm width. The single dissipative particle here is of the order of 10 nm and the total number of dissipative particles is 10800. As it can be seen from Fig. 4 the velocity corresponds to that one of the continuum prediction. It should be emphasized that all particles in the flow are shown as the presentation is not a cross-section or result of an averaging procedure. The particles aligned with the flow one behind another, therefore all cross-sections would look identical. The density and entropy, are not plotted, but for this case there are straight lines with the same constant value and there is no jump in the vicinity of the wall boundaries. The main conclusion for this first test is that the continuum scale is resolved correctly even in the range of nano-meters. However, this computations did not involve fluctuation term, which as was indicated earlier is important for mesoscale liquids.

The influence of the fluctuations on the channel flow can be seen in Fig. 5a. The plot represents velocity in the y-direction. The line in the middle refers to the continuum flow for which fluctuation is not included. All remaining points correspond to the same channel flow with fluctuations. For this case fluctuations in y-velocity are three orders of magnitude smaller than the velocity in x-direction. Hence, the general velocity profile will not be affected by fluctuations. However, for smaller flow velocities this tendency will change. Second part of the Fig. 5 shows the difference in y-velocity fluctuations for three different channel geometries. First one is as the one above, second is 10 times larger in each direction – 1.5 μm × 0.9 μm and the third is 15 μm × 9 μm. As it was expected Brownian motion of the particles depends on the mass and heavier particles will have smaller fluctuations. Another conclusion from the figure is that the centre of the channel seems to be affected less by fluctuations than regions near the boundary. This is due to the flow reinforcement and actually will have the influence on the immersed structures behaviour, which will be discussed in details later.

Figure 5 confirms the fact that the Brownian particles (example dissipative particle form computations) move slower when they are heavier. However, the mean velocity of the drift should stay the same. This is due to the fact that the mean displacement defines self-diffusion coefficient. To estimate the self-diffusion coefficient of the particles another test was performed. Equations 21 and 22 provide information about fluctuation. However, the precise value of the term is estimated based on the fluctuation-

dissipation theorem. In macroscopic description it usually presents itself as a relation connecting fluctuating terms with dissipative part. Equation 1 can be considered as a one of the very simple example. It connects random fluctuations with the macroscopic parameter of self-diffusion coefficient. Another example of fluctuation-dissipation relation is
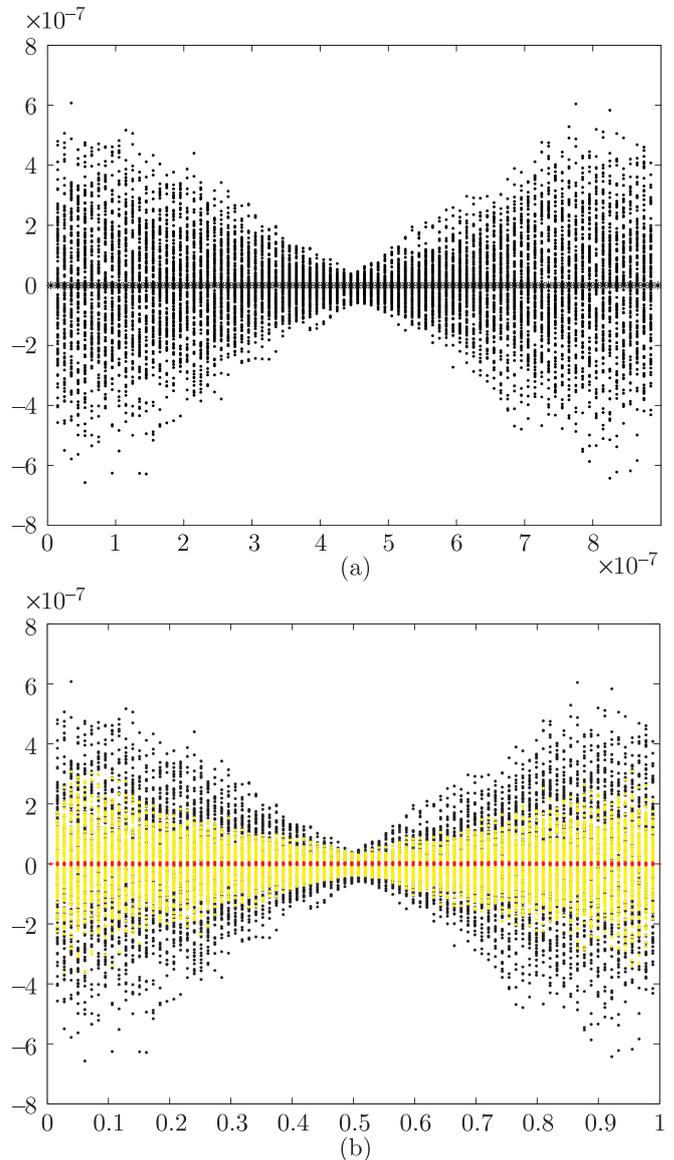
$$D = \frac{k_B T}{6\pi \eta R}, \qquad (24)$$

Fig. 5. Channel flow with fluctuations; a) Velocity in y-direction in the function of y-coordinate, middle line corresponds to flow without fluctuations, the dots are representing the same case with fluctuating term; b) Velocity in y-direction in the function of y-coordinate (normalized to the channel width). The middle line represents the largest channel, 15 μm × 9 μm, light points – 1.5 μm × 0.9 μm, black dots – 1200 nm × 900 nm

which relates random motion to the viscous effects. The Dissipative Particle Dynamics formulation have different fluctuation-dissipation theorem (details are in [34,35]),

which ensures momentum and energy conservation. However, the fluctuation-dissipation theorem also provides several other physically significant points. From the microscopic point of view fluctuation will be present in the system in thermodynamical equilibrium. Onsager has proven that the system response to the external perturbation is correlated with the equilibrium fluctuations. The diffusion coefficient obtained from studying the equilibrium correlations is the same as the one in continuum models for time scale sufficiently longer than relaxation time. Hence, the fluctuation-dissipation theorem will ensure that for long time scale the self-diffusion coefficient is constant. Moreover, the speed of sound waves, as a response of the system to the external perturbation, will also be controlled by the fluctuation-dissipation theorem. Thus, Eqs. 1 and 3 are indeed representing similar phenomena connected to the response of the system to the perturbation. This leads to the realization that correct calculation of the speed of sound especially on the short time scales is crucial for the micro-liquids. To ascertain if the model presented here is correctly behaving in the presence of disturbance, the following simulation is performed. The box 10 μm × 10 μm with 1600 particles of water was initially perturbed with small force and than the behaviour of the mean particle drift was studied. Figure 6 presents the drift behaviour over time. As it was expected in the liquid without fluctuations the diffusion coefficient based on the particle drift is zero. This occurs after time, when initial disturbance was dumped. The liquid with fluctuations behaves differently. Firstly, the very short time scale, shows that the motion of the particles is uncorrelated and its initial rise corresponds to the one which is obtained from the simple Langevin equation, example in [20]. However, longer times lead to correlation between particles and this shows in the plateau. For very long time, however, the constant diffusion coefficient is recovered. It has to be mentioned, that conservation of the mass does not have the fluctuation term. The influence is indirect, through the momentum and entropy equations. Hence, in general the self-diffusion effects can be estimated correctly without mass exchange between particles. In the simulations one of the curved represents the behaviour, for particles when mass changes are not allowed. In such a case the diffusion coefficient is larger to compensate mass transfer effects. The diffusion coefficient can be calculated from 24 - $2.19 \cdot 10^{-14} \mathrm{m}^2/s$ and for both cases is in the range of the theoretical prediction for spherical particles ($1.85 \cdot 10^{-14} \mathrm{m}^2/s$; $1.03 \cdot 10^{-14} \mathrm{m}^2/s$). Hence, the diffusion processes for the small time scales are represented correctly by fluctuation-dissipation theorem and for the long time the value is ensured by continuum approach.

Another aspect which should be considered is if the time scale between diffusion and viscous process is resolved correctly. This will be especially important for molecular mixing processes. However, as can be noted from the Schmidt number definition 1, if viscosity and

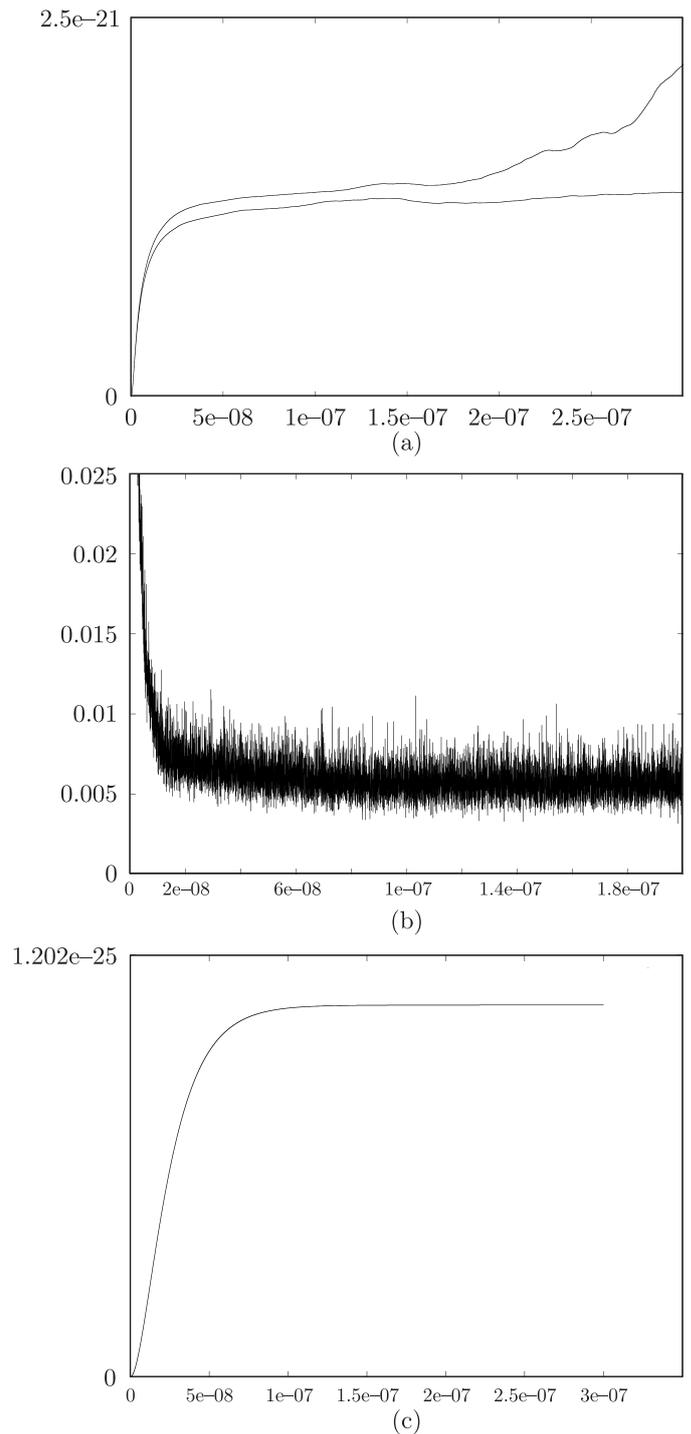self-diffusion coefficient are known and resolved correctly, the time scale is then estimated correctly.

Fig. 6. Response of the liquid to the small perturbation. (a) two cases, one in which the mass transfer between particles was not allowed (higher curve) and second when the mass transfer was present; (b) average mass changes between particles; (c) the continuum equations without fluctuation term

Finally, after estimating the size of fluctuations and the relevant time scale, the remaining question is then to ascertain the importance of diffusion processes for mesoscale liquids. From the channel flow above with velocity $V_x = 10^{-4}$ m/s and Reynolds number based on the

channel length $Re = 10^{-4}$ the size of fluctuation remains fairly small. Hence, it seems that the fluctuations after all might not be of primary importance for many engineering applications. The Reynolds number is usually much larger and the one of the order of 10^{-7} would be difficult to obtain. However, this is very misleading. The fluctuation impact depends on the space/time scales relation and the mass of the particle. One of the cases, which is very interesting for bioengineering application is the manipulation of DNA molecules. As it will be shown below for such application self-diffusion effects will influence process significantly.
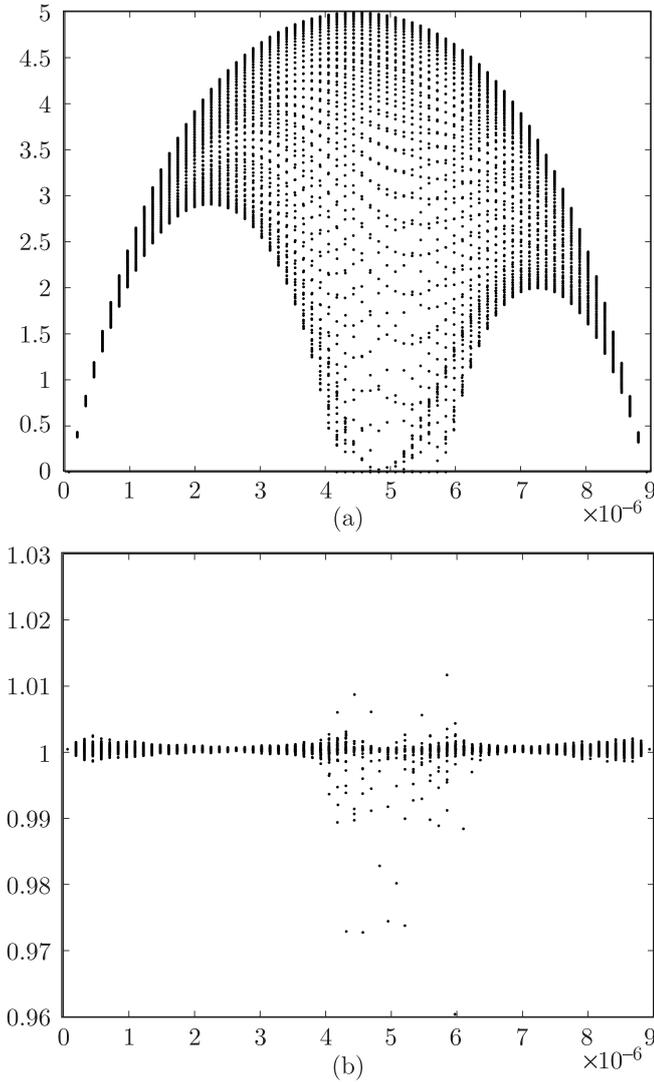

(a)

(b)

Fig. 7. Channel flow with the DNA chain; a) x-Velocity in the function of y-coordinate; all particles are plotted. Main flow maintain parabolic profile far from the DNA; normalized mass in the function of y-coordinate; all particles are plotted

5.1. Immersed structures in the flow and Brownian effects.
A case study to examine the influence of the Brownian effects on the immersed structure is performed by considering the channel flow with DNA chain. Most of the experimental studies are concerned with stretching

of the DNA, as exemplified in [38–41]. However, here the importance of the of the flow structures on the stretching process will be underlined. Due to the fact that, the consideration are restricted to the estimation of self-diffusion effects in liquids, the simple model of DNA is sufficient for such a case study. In general, DNA – fluid interaction is modelled on the atomistic level and the mesoscale description is highly simplified and do not take to account various important phenomena [42]. The mesoscale DNA model presented here will be combination of the Dissipative Particle Dynamics and classical FENE approach, and the way to obtain it is by similar patter as it is performed in the Brownian Dynamics simulations, example in [43].

To model polymer the non-Hookean FENE spring model was chosen. The force is obeying relation

$$\mathbf{F}^{FENE} = \frac{H\mathbf{L}}{1 - (L/L_0)^2}, \tag{25}$$

where H is spring constant. The spring cannot extend beyond $L_0^2 = 1.2\, l^2$, l is the initial length. The mass centres are associate with every Voronoi centre and the deformation follows similar rules as the one for dissipative particle.

The position of the each bead is calculated similarly to the Ermak-McCammon algorithm differentiating Langevin equation in high friction limit, where inertia term are neglected. In our case inertia term will be result of the DPD integration and will be implicitly influencing behaviour of the polymer

$$\mathbf{r}_i = \mathbf{r}_i^0 + \frac{\Delta t}{kT} \sum_j \mathbf{D}_{ij}^0 \cdot \mathbf{F}_{\mathbf{j}}^{\mathbf{0}} + \mathbf{v}_i^0 \cdot \Delta t, \; i = 1, .., N. \tag{26}$$

Generally the chain-solvent interaction is approximated by the fluctuation part. However, the fluctuation term is not explicitly present to affect deformation by the velocity of the Dissipative Particle. Such formulation ensures that diffusion effects influencing DNA are indeed the same as modelled in liquid. The diffusion tensor for deformation part is as presented

$$\mathbf{D}_{ii}^{(\alpha\beta)0} = \frac{kT}{\zeta}\, \delta_{\alpha\beta}, \;\; i = 1, .., N;$$
$$\mathbf{D}_{ij}^{(\alpha\beta)0} = 0, \;\; i \neq j = 1, .., N; \tag{27}$$

where viscous friction is related to fluid viscosity as

$$\zeta = 6\pi\eta\, 0.257l. \tag{28}$$

There is another assumption made in considering the stretching mechanism. If the stretched length is much longer than the maximum length, the DNA should break. However, in the current simulation, the DNA will stay in fixed position, when stretched to its material property limit. The assumption was made to avoid considerations regarding the material properties in the DNA stretching mechanism. There are several issues considering DNA modelling, which require detailed studies that are beyond scope of this paper.

To estimate Brownian motion effects following simulations were performed. Channel flow 1.2 μm × 0.9 μm

with 6300 particles and the DNA is constructed from the 87 of Voronoi particles. The Reynolds number based on the channel length is $6 \cdot 10^{-5}$. Accordingly to the Eq. 3 the fluctuations will affect time scales around 10^{-9} s. A time step was chosen accordingly as 10^{-10} s, and the total time was 4000 time step.
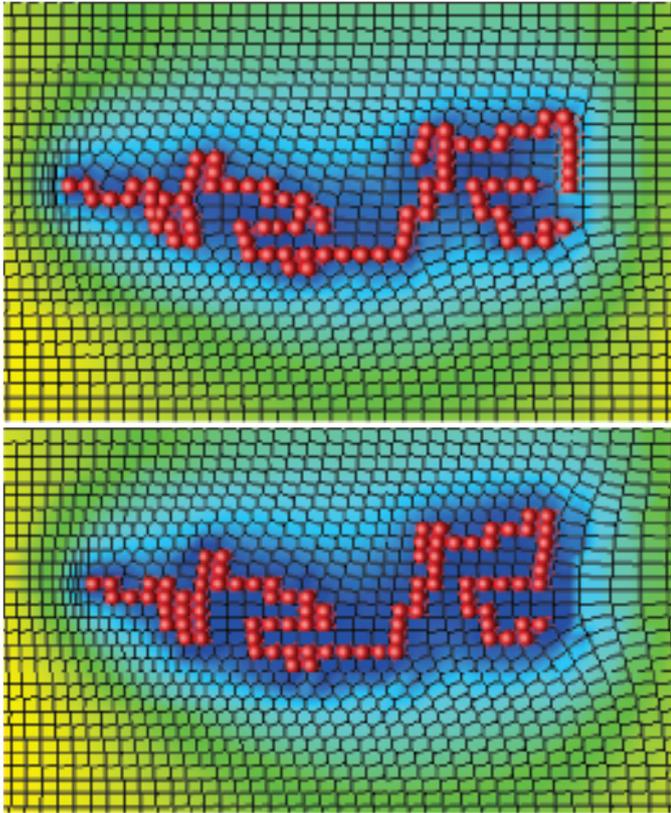

Fig. 8. Velocity distribution in the channel flow during the DNA stretching procedure. The DNA is attached by fixing the position of the first particle on the left end of the chain. Top picture represents case without fluctuations. Bottom picture shows the same flow with the Brownian effects enhancing the DNA stretching procedure

Figure 7 presents the example of x-velocity in the function of y-coordinate profile for all particles in the channel. It can be seen that parabolic profile is recovered in the global channel, as well as in the flow between DNA. The presence of the DNA influences the changes of the mass of the particles 7, however the effect is connected to the numerical error and more information about this can be found in the appendix. Figure 8 shows the velocity field for two cases : top one is for without fluctuations and the bottom, includes stochastic interaction. As it can be noted, global velocity field is very similar, however there are significant differences in the vicinity of the DNA chain. The main difference is for non-Brownian flow the stretching is mostly performed in the direction of the flow. The deformation is smaller, however the stretching length is about the same as for the Brownian motion influenced DNA chain. The differences in the behaviour can be seen even more clearly in Fig. 9. The first part presents

instantaneous resultant x-displacement for every bead of the chain. As it can be seen, the Brownian effects increase movement of the DNA significantly. The second part of the figure presents the average displacement of the chain in the flow in the function of time. The average displacement should be a function of the mean flow velocity, hence both curves have similar profile. However, there is significant difference in the behaviour of both cases. The plot could be considered as a estimation of the diffusion constant of the polymer. However, the flow is enforced and the average displacement also is influenced by the flow itself. Therefore, for the estimation of the diffusion coefficient for this case the equation from [42] will be used. The relation between diffusion coefficient of the monomer particle D_m and polymer chain D_p is

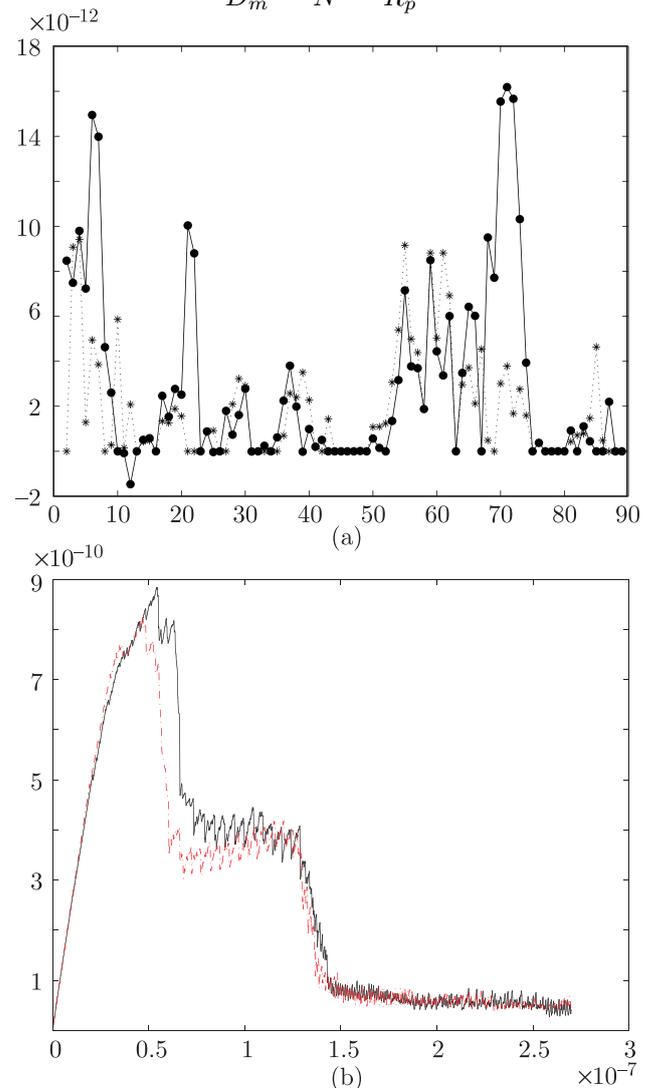$$\frac{D_p}{D_m} = \frac{1}{N} + \frac{R_m}{R_p}, \qquad (29)$$

Fig. 9. The influence of the fluctuations on the DNA stretching procedure; a) the instantienous plot of the x-direction displacement for the time $3 \cdot 10^{-7}$s as a function of the particle number in the chain; stars – correspond to the case without fluctuations; circles – displacement with the fluctuations; b) the time evolution of the mean displacement; red, dotted line – flow without fluctuations, black – flow with fluctuations

where N is the number of the bead, R_m the radius of the monomer particle, R_p – radius of the polymer. This relation leads for the DNA case to ratio $D_p/D_m = 0.048$. This again confirms the fact that heavier Brownian particles is affected by smaller fluctuations. However the average displacement still remains significant, as the DNA-liquid interaction is reflected in the second part of the equation. Hence, the liquid self-diffusion coefficient will have dominating influence on the long polymer chains.

6. Conclusions

This paper presents a new modelling approach for simulating mesoscale phenomena in liquids. As it was shown on such a scale the self-diffusion related effects are predominant. Various important nano- and bioengineering applications need to resolve such phenomena, example molecular mixing, manipulation of polymers or cells. However, the understanding of following process is still in progress. Experimental approach in some cases, do not provide complete information. For example, on nano-meter scale, there is difficulty in obtaining the information about the flow field phenomena. Hence, a realistic numerical simulation can provide crucial help in bridging the experimental information gap. However, there are very few numerical methods, which can efficiently cope with this task. Here, the Voronoi Dissipative Particle Dynamics was presented with a very satisfying result. The imposing of flux boundary condition on the fluid-solid interface and Voronoi adaptivity has significantly reduced density jump on the boundaries, which is present in many particle methods and which alters significantly flow structure.

Mesoscale phenomena are the resultants of two major effects in liquids, namely the intermolecular potential and random molecular drift. Both of these aspects help to define the mesoscale borders and also need to be resolved correctly by any numerical approach. Voronoi Dissipative Particle Dynamics, due to the fact that the Schmidt number is similar to that one of the real liquids, models the processes accurately and in very efficient way. The presented method, due to the fact that the the time averaging is not require to obtain the flow field is few order of magnitude faster than other applications of DPD.

It was shown that self-diffusion effects can influence flow in various ways. In some cases such as channel flow, the fluctuations do not play an important role. However, in the presence of any immersed structure the situations change drastically. As a example the DNA chain stretching case was chosen. The fluctuation influence alters significantly this procedure.

Appendix

Numerical procedure, accuracy and efficiency.

There are several issues related to the numerical procedure. First is related to the movement of the Voronoi

lattice. Voronoi diagram is a tool to describe proximity of neighbouring points $U = P_1, ..., P_n$. The perpendicular bisector is defined as

$$B_{ij} = \{\, x \in \Re^2 \mid d(x, P_i) = d(x, P_j)\,\}, \qquad (A1)$$

where $d(x, P_i)$ is the distance between any point x and Voronoi center P_i. The Voronoi polygon of P_i is defined as

$$V(\mathbf{P}_i) = \{\, x \in \Re^2 \mid \forall_{i \neq j}\ d(x, P_i) \leq d(x, P_j)\,\}. \qquad (A2)$$

Set of Voronoi points defines Voronoi diagram, dual graph to the Delaunay triangulation. Due to the movement of Voronoi centres the diagram requires reconstruction. Two assumptions are important: first that points do not collide and second that initial diagram is actually a Voronoi diagram. In such a case there are three types of events. The appearance (or disappearance) of additional Voronoi point in the neighbouring vicinity of point P_i. If the point P_i is on the wall, therefore does not move or is on the periodic boundary, in such case the mirror image of point P_i is created. Therefore the problem is confined to consideration of movement of the Voronoi lattice on the torus. It can be shown that the change in the Voronoi lattice is characterized by topological diagram shown in Fig. 11.
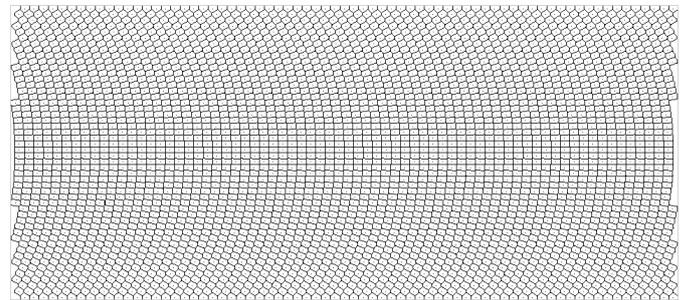

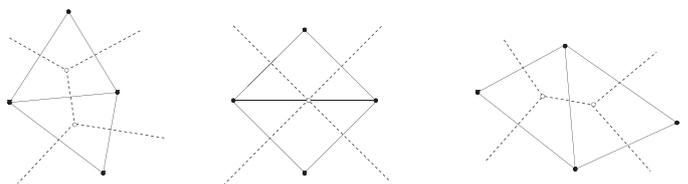Fig. 10. Deformation of particles in the channel flow (3500 particles)

Fig. 11. Topology changes in the four neighbouring Voronoi cells (dotted line). Changes in Delaunay triangulation are also presented. The flip procedure causes that two Voronoi are gaining new neighbour and other two are loosing one neighbour. The middle graph represents the degenerate case, which is the topological state, but does not actually appear in practice

Hence, the updating of the diagram only requires reconstruction partially in the cells, which are influenced by the changes. It can be proven that the algorithm efficiency is $O(n + F \log n)$, where F is the number of flips. The efficiency of the complete reconstruction of Voronoi diagram in 2D is $O(n \log n)$, so for a large amount of flip cases the reconstruction of the whole diagram can be similarly efficient. However, for the DPD application usually

time step is limited by entropy grow and the changes of particles size are small, requires very few flips (less than 5%) in every time step.

More details about the construction of moving Voronoi diagram can be found in [44].
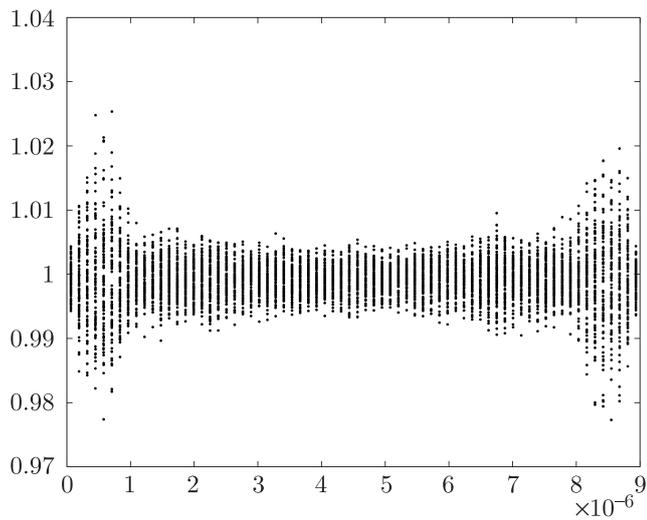

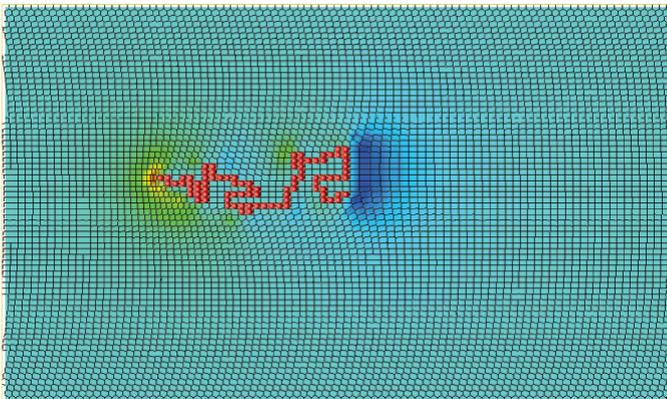Fig. 12. Mass change due to the Voronoi lattice motion

Fig. 13. DNA in the channel flow. Changes in density due to the adaptation of the volume of the particles to the flow structures

The example of the particle deformation in a channel flow is given in figure 10. It should be noted that the movement of the particles depends on the flow velocity. Thus, for a given geometry, in some cases the mesh will deform more and in other cases, they will stay mostly in the original position. The original mesh is build from equally distributed points, which are slightly perturbated to obtain Voronoi diagram. In the case of channel flows presented in the paper the mesh did not deform noticeably. The disadvantage of the deformation is that the accuracy of the integration is lower and the numerical error increases. Example is given for the channel flow, for the same channel geometry which was considered for DNA flow, except that DNA chain is not present. The time is 4 times longer than DNA simulation. Figure 12 presents changes in the normalized mass of the particles in the

presence of extensive motion. It needs to be indicated that it is strictly numerical error and can be reduced to any small value by reducing the time step size. However, for the flow with the DNA chain the extensive deformation makes the changes in the DNA position faster. Hence, the compromise has to be determined between accuracy requirement and the desired speed of considered process. Next computational issue is related to the boundary conditions. Classical Dissipative Particle Dynamics represent no-slip boundary condition with the frozen particle layer. However, it leads to clustering of particles in the vicinity of the boundaries and this is responsible for large density jump. To model wall boundary condition also frozen particles layer was assumed. However, the mass exchange between particles is allowed, as does entropy change. This leads to very different result than the one obtained in many particle methods. The boundary is represented accurately, and there is no density jump. However, when the immersed structures are present, some complex flow patters cause density changes. The mass as it was shown in Fig. 7b) does not change significantly, but the volume of the particles does. This can be seen in Fig. 13. This numerical inconvenience can be reduced by imposing certain rules on the particle splitting or creation in the vicinity of stagnation and wake region.

Another computational issue is related to the channel flow, for which periodic boundary conditions were imposed and the flow was driven by the force. Periodic boundary is represented in the way that the Voronoi edge nodes have the same index, however two different actual positions. The nodes, however have one position and only communicate fact that some neighbours may have distant position. This leads to the fact, that there are no extra ghosts cells in the system and all particle seen on figures are indeed the all particles of the fluid.

Finally, remaining issue considers time integration and algorithm efficiency. For the time integration Runge-Kutta method was used. Due to the fact that the Schmidt number is of the same order as real fluids, stochastic part in many cases is very small. Hence, the integration error for that part is small as well. In the case when the fluctuation term is larger the appropriate stochastic integration scheme should be used. The stability of the algorithm is estimated by the two factors $\mathbf{\Gamma}_{ij}$ and $\mathbf{\Omega}_{ij}$. Parameter $\mathbf{\Gamma}_{ij}$ indicates changes in the shape of the Voronoi cells, while $\mathbf{\Omega}_{ij}$ is related to the relative movement of the mass centres of two interacting particles. Due to the fact that the conservation of mass 18 needs to be fulfilled with as small error as possible the parameter $\mathbf{\Gamma}_{ij}$ will restrict the time step. Reversible part will be determining the time step, also when the irreversible processes are present. However, parameter $\mathbf{\Omega}_{ij}$ determines how many time steps are needed to obtain fully developed flow profile. Hence, the difference between these two parameters is responsible for the fact that in some cases the mesh moves extensively and in some the flow can be established without noticeable deformation of Voronoi lattice.

Time efficiency can be also studied from the different aspect. Schmidt number has influence not only on the physical aspect of the flow. It determines how easily the flow structures can be obtained. In case presented in [28] to obtain channel flow $2.5 \, 10^7$ timesteps were needed (2500 timesteps and every time step was averaged over 10^4 timesteps) with the calculations performed without energy conservation. The energy equation makes particles more mobile, example in [29] and requires even longer averaging. Here, however the flow in some cases can be obtained after as low as 4000 timesteps with the same amount of particles (10800) and this include energy equation. Thus, despite of inconvenience in requirement for the move of the complex geometrical structures such as Voronoi cells, the method is very time efficient.

REFERENCES

[1] M. Gad-el-Hak, "The fluid mechanics of microdevices the freeman scholar lecture", *J. Fluids Eng.* 121, 533 (1999).

[2] H. Herwig, "Flow and heat transfer in micro systems: is everything different or just smaller?", *Z. Angew. Math. Mech.* 82, 579586 (2002).

[3] K. Pohl, M.C. Bartelt, J. de la Figuera, N.C. Bartelt, J. Hebek, and R.Q. Hwang, "Identifying the forces responsible for self-organization of nanostructures at crystal surfaces", *Nature* 397, 238241 (1999).

[4] W. Dzwinel and D. A. Yueny, "A two-level, discrete-particle approach for simulating ordered colloidal structures", *J. Coll. Interf. Sc.* 225, 179190 (2000).

[5] I. Aranson, S.B. Meerson, P.V. Sasorov, and V.M. Vinokur, "Phase separation and coarsening in electrostatically driven granular media", *Phys. Rev. Lett.* 88, 204301–204314 (2002).

[6] A.A. Darhuber and S.M. Troian, "Principles of microfluidic actuation by modulation of surface tension", *Annu. Rev. Fluid Mech.* 37, 425455 (2005).

[7] C.-M. Ho and Y.-C. Tai, "Micro-electro-mechanical-systems (MEMS) and fluid flows", *Annu. Rev. Fluid Mech.* 30, 579612 (1998).

[8] H.A. Stone, A.D. Stroock, and A. Ajdari, "Engineering flows in small devices: microfluidics towards a lab-on-a-chip", *Annu. Rev. Fluid Mech.* 36, 381411 (2004).

[9] S. Senapati and M.L. Berkowitz, "Computer simulation study of the interface width of the liquid /liquid interface", *Phys. Rev. Lett.* 87 (17), 176101–176114, (2001).

[10] C. Denniston and M. O. Robbins, "Molecular and continuum boundary conditions for a miscible binary fluid", *Phys. Rev. Lett.* 87 (17), 178302–178314 (2001).

[11] A. Jabbarzadeh, J.D. Atkinson, and R. I. Tanner, "Effect of the wall roughness on slip and rheological properties of hexadecane in molecular dynamics simulation of Couette shear flow between two sinusoidal walls", *Phys. Rev. E* 61 (1), 690699 (2000).

[12] M. Cieplak, J. Koplik, and J.R. Banavar, "Boundary conditions at a fluid-solid interface", *Phys. Rev. Lett.* 86 (5), 803806 (2001).

[13] M. Knott and I.J. Ford, "Surface tension and nucleation rate of phases of a charged colloidal suspension", *Phys. Rev. E* 65, 061401–061413, (2002).

[14] D.E. Smith, H. P. Babcock, and S. Chu, "Single-polymer dynamics in steady shear flow", *Science* 283, 17241727 (1999).

[15] R.J. Davenport, G.J.L. Wuite, R. Landick, and C. Bustamante, "Single-molecule study of transcriptional pausing and arrest by E. coli RNA polymerase", *Science* 287, 24972500 (2000).

[16] W.K. Kegel and A. van Blaaderen, "Direct observation of dynamical heterogeneities in colloidal hard-sphere suspensions", *Science* 287, 290293 (2000).

[17] D. Nykypanchuk, H.H. Strey, and D.A. Hoagland, "Brownian motion of DNA confined within a two-dimensional array", *Science* 297, 987990 (2002).

[18] J. van der Gucht, N.A.M. Besseling, W. Knoben, L. Bouteiller, and M.A. Cohen Stuart, "Brownian particles in supramolecular polymer solutions", *Phys.Rev. E* 67, 051106–051110 (2003).

[19] A.E. Pelling, S. Sehati, E.B. Gralla, J.S. Valentine, and J.K. Gimzewski, "Local nanomechanical motion of the cell wall of Saccharomyces Cerevisiae", *Science* 305, 11471150 (2004).

[20] J.-L. Barrat and J.-P. Hansen, *Basic Concepts for Simple and Complex Liquids*, Univ. Press, Cambridge, 2003.

[21] P. Koumoutsakos, "Multiscale flow simulations using particles", *Annu. Rev. Fluid Mech.* 37, 457487 (2005).

[22] H. Brenner, "Is the tracer velocity of a fluid continuum equal to its mass velocity?", *Phys. Rev. E* 70, 061201–061210 (2004).

[23] S. Chen and G.D. Doolen, "Lattice Boltzmann method for fluid flows", *Annu. Rev. Fluid Mech.* 30, 329364 (1998).

[24] A.J.C. Ladd, "Short time motion of colloidal particles: Numerical simulations via a fluctuating lattice Boltzmann equation", *Phys. Rev. Lett.* 70, 1330–1342 (1993).

[25] P.J. Hoogerbrugge and J.M.V.A. Koelman, "Simulating microscopic hydrodynamics phenomena with dissipative particle dynamics", *Europhys. Lett.* 19, 155160 (1992).

[26] C.L. Henry, C. Neto, D.R. Evansa, S. Biggs, and V.S.J. Craig, "The effect of surfactant adsorption on liquid boundary slippage", *Physica A* 339, 6065 (2004).

[27] R.D. Groot, "Application of dissipative particle dynamics", *Lect. Notes Phys.* 640, 538 (2004).

[28] X. Fan, N. Phan-Thien, N.T. Yong, X.Wu, and D. Xu, "Microchannel flow of a macromolecular suspension", *Phys. Fluids* 51, 1121 (2003).

[29] U. Salecker, J. Czerwinska, N.A. and Adams, "Modelling of micro-cavity flow ba a Dissipative Particle Dynamics method", *Proceed. GAMM* (2004).

[30] C.P. Lowe, "Alternative approach to dissipative particle dynamics", *Europhys. Lett.* 47, 145151 (1999).

[31] J. Bonet Avalos and A.D. Mackie, "Dissipative particle dynamics with energy conservation", *Europhys. Lett.* 40, 141146 (1997).

[32] X.F. Yuan, R.C. Ball, and S.F. Edwards. "A new approach to modelling voscpelastic fluid flows", *J. Non-Newtonian Fluid Mech.* 46, 331350 (1993).

[33] E.G. Flekkøy and P. V. Coveney, "From Molecular Dynamics to Dissipative Particle Dynamics", *Phys. Rev. Lett.* 83, 17751778 (1999).

[34] E.G. Flekkøy, P.V. Coveney, and G. De Fabritiis, "Foundations of dissipative particle dynamics", *Phys. Rev. E* 62, 21402157(2000).

[35] M. Serrano, G. De Fabritiis, P. Español, E. G. Flekkøy, and P.V. Coveney, "Mesoscopic dynamics of Voronoi fluid

particles", *J. Phys. A: Math. Gen.* 35, 16051625 (2002).

[36] M. Serrano and P. Español, "Thermodynamically consistent mesoscopic fluid particle model", *Phys. Rev. E* 64, 046115–046118 (2001).

[37] H. C. Öttinger, "General projection operator formalism for the dynamics and thermodynamics", *Phys. Rev. E* 57, 1416 (1999).

[38] A. Crut, D. Lasne, J.-F. Allemand, M. Dahan, and P. Desbiolles, "Transverse fluctuations of single DNA molecules attached at both extremities to a surface", *Phys.Rev. E* 67, 051910-051916 (2003).

[39] P.S. Doyle, E.S.G. Shaqfeh, and A. P. Gast, "Dynamic simulation of freely draining flexible polymers in steady linear flows", *J. Flid Mech.* 334, 251291 (1997).

[40] R.M. Jendrejack, E.T. Dimalanta, D.C. Schwartz, M.D. Graham, and J.J. de Pablo, "DNA dynamics in a microchannel", *Phys. Rev. E* 91 (3), 038102-038114 (2003).

[41] B. Ladoux and P. S. Doyle, "Stretching tethered DNA chains in shear flow", *Euro Phys. Lett.* 52, 511517 (2000).

[42] C.P. Lowe and M.W. Dreischor, "Simulating the dynamics of the mesoscopic systems", *Lett. Notes Phys.* 640, 3968 (2004).

[43] A.V. Lyulin, D.B. Adolf, and G.R. Davies, "Brownian dynamics simulations of linear polymers under shear flow", *J. Chem. Phys.* 111 (2), 758771 (1999).

[44] G. Albers, J.S.B. Mitchell, L.J. Guibas, and T. Roos, "Voronoi diagram of moving points", *3rd SWAT 92* (1992).